A STATIC ACOUSTIC SIGNATURE SYSTEM FOR THE ANALYSIS OF DYNAMIC FLIGHT INFORMATION

DANIEL J. RAMER
U.S. ARMY ARMAMENT RESEARCH AND DEVELOPMENT COMMAND

SUMMARY

The Army family of helicopters was analyzed to measure the polar octave band acoustic signature in various modes of flight. A static array of calibrated microphones was used to simultaneously acquire the signature and differential times required to mathematically position the aircraft in space. The signature was then reconstructed, mathematically normalized to a fixed radius around the aircraft.

INTRODUCTION

A number of years ago, this organization was asked to measure the polar octave band output of each of the Army family of helicopters in various modes of flight. The intent was to, first, model the perception, based on this signature study, of an unsophisticated enemy force who would be expected to fire on friendly aircraft with small arms and, second, predict and minimize attrition based on flight tactics. Since each aircraft was to be traveling at some considerable velocity during data acqusition, some means of measuring the output through 360 degrees had to be devised. Emplacing a circular array of microphones was rejected as was towing a microphone behind a lead aircraft. It was decided to combine this organization's sound ranging techniques with signature analysis to mathematically construct the desired family of polar signatures.

This paper, then, will describe the application of a measurement technique normally restricted to transient phenomena to that signature task.

SYMBOLS

c	velocity of sound
L	distance between any two adjacent microphones
n_1	differential propagation distance between first and second excited microphones
n_2	differential propagation distance between first and third excited microphones
R	radial distance between origin microphone and sound source
V_s	velocity of propagation
V_w	vector average of wind velocity during sound propagation
x	one cartesian distance between origin microphone and sound source
y	remaining cartesian distance between origin microphone and sound source
δ	propagation medium shift
Δt_{12}	differential time between first and second excited microphones
Δt_{13}	differential time between first and third excited microphones

THE THEORY AND APPLICATION OF SOUND RANGING

Sound ranging is a technique which can be used to accurately determine the location of an impulsive sound source in three-dimensional space. This technique was developed to measure munition performance in jungle canopy where radar and optical techniques are impractical.

To implement sound ranging data acquisition, a geometric array of microphones is emplaced in a surveyed position at a target site. The shape of the array was determined by error analysis of various mathematical models.

A typical array consists of from 3 to 6 microphones, although any number greater than three could be used. Sound emanating from the source propagates through the air at a relatively constant velocity, and the wave-front arrives at each microphone at a specific time after the sound has occurred. The differences in arrival time among the various microphones are accurately determined. Equations, derived from the Euclidean geometry, the velocity of sound, and the differential times between the microphones, will yield the position coordinates of the sound source.

A typical two-dimensional sound ranging transducer array is shown in figure 1. For this transducer system, the mathematical solution can be obtained from the geometry as follows:

$$R^2 = x^2 + y^2 \tag{1}$$

$$(R + n_1)^2 = x^2 + (L - y)^2 \tag{2}$$

$$(R + n_2)^2 = x^2 + (2L - y)^2 \tag{3}$$

expanding (2) and (3) and substituting (1) for x,

$$R^2 + 2Rn_1 + n_1^2 = R^2 - y^2 + L^2 - 2Ly + y^2 \tag{4}$$

$$R^2 + 2Rn_2 + n_2^2 = R^2 - y^2 + 4L^2 + y^2 - 4Ly \tag{5}$$

which reduces to

$$2Rn_1 + n_1^2 = L^2 - 2Ly \tag{6}$$

$$2Rn_2 + n_2^2 = 4L^2 - 4Ly \tag{7}$$

solving for R from (6)

$$R = \frac{(L^2 - 2Ly - n_1^2)}{2n_1} \tag{8}$$

substituting in (7)

$$2\,\frac{(L^2 - 2Ly - n_1^2)}{2n_1}\, n_2 + n_2^2 = 4L^2 - 4Ly$$

solving for y

$$y = \frac{L^2 (4n_1 - n_2)\ (n_1 n_2) + (n_1 n_2)}{2L\ (2n_1 - n_2)} \tag{9}$$

Substituting this value of y in (8) yields R and substituting R and y in (1) yields x.

A second array, either parallel or perpendicular to the first, yields a second set of coordinates which are combined with the first set to derive the third dimensional distance, z.

There are significant sources of error with this approach, however. Signal-to-noise and resolution errors can be a problem but, since these are related to the nature of the specific acoustic signature produced by the test item, for the purposes of this paper will not be discussed. That leaves the assumption that the velocity of sound is constant, which of course, it is not. Wind and wind gradients and, to a lesser extent, temperature gradients will all distort the velocity of propagation. Wind, more properly, represents the migration of the total medium during propagation, but for the purposes of error analysis can be considered a propagation velocity shift (figure 2).

In figures 3 and 4, the errors in x and y induced by a 1% error in the velocity of propagation are shown. After a first glance, there is a tendency to structure the test to place the microphones at several times the microphone array dimension from the test item to minimize this type of error; however, in reality, the larger this distance, the more appreciable velocity gradients will become. Thus the trade-off must be made between improved accuracy in constant wind velocity, against reduced accuracy caused by topographically induced wind gradients.

An error correcting scheme for wind has been devised; computer modeling indicates accuracy improvements of up to an order of magnitude result. Briefly, this technique involves the storage of total vector anemometer history, the computation of position coordinates based on a constant propagation velocity, the reconstruction of propagation velocity based on wind data over the computed distance, the recomputation of coordinates based on the new velocity of sound, and the reconstruction and recomputation repeated until the result is converged upon. The tolerance between successive recomputations determines the exit from the algorithm.

The hardware necessary to execute this technique include total vector anemometers, microphones, line drivers, transient recorders, time code generator and digital processor (figure 5). This system is designed to store data and compute the coordinates of a transient forcing function. The techniques, however, are applicable to repetitive transient producing vehicles, such as helicopters.

APPLYING SOUND RANGING TO HELICOPTERS

Having been given the task of measuring the polar signature around an aircraft in flight, it was decided to fly the aircraft by a sound ranging array of calibrated microphones to simultaneously acquire the signature and position information. A magnetic tape medium was selected since the Real-Time Sound Ranging System was incapable of keeping up with the data rates. A data processing scheme was devised to compute the position of the aircraft in polar coordinates, measure the rms amplitude of each octave band, correct those amplitudes for spreading loss and absorption, and finally, list the polar distributions of octave band energy.

Clearly, this methodology depended on the ability to distinguish a long wavelength repetitive phenomenon in the acoustic signature of each aircraft to utilize sound ranging; and, conveniently, the helicopter blade slap provided just such a waveform. A Huey Cobra, for example, will typically produce a blade slap rate of 14Hz, a Huey approximately 12Hz. Thus, with fundamental wavelengths in excess of 23 meters, a substantially sized microphone array could be surveyed in place. This permitted acceptable accuracies over the distances required to measure the aircraft signatures at low angles of incidence. Further, those long wavelengths avoided the necessity of keeping track of multiple cycles when the wavelength is exceeded by the inter-microphone distances.

This data acquisition and reduction task was greatly simplified by the funding organization's request to operate in still air, for in addition to the instrumentation, accompanying personnel took part in simultaneous threshold perception tests.

Figure 6 illustrates the reduction hardware. To accurately range the aircraft during data reduction, it was necessary to insure differential time measurements between the same point on each succeeding cycle of acoustic signature. Thus, phase lock loops were utilized to lock onto the fundamental blade slap frequency transduced by each microphone. Each channel from the magnetic tape recorder drove a phase lock loop; the lock range was adjusted to a reasonable range around the fundamental blade slap frequency for each aircraft and the loop time constant made long, approximately 1 sec, to "flywheel" over dropouts caused by topographical multipath, the tape medium or air turbulence. The square wave output of each phase lock loop was differentiated to yield a pulse of 100 μsec in width which, in turn, drove both the stop and start enable ports of each counter and the first-in start logic.

The first-in start logic generated a start pulse for each counter only when it received a pulse from the first arrival microphone circuitry. It then counted the remaining microphone outputs and started over again; since this circuit produced a 50 μsec wide pulse, the counter associated with the first excited microphone always read zero. The start logic also contained sequencing logic that would permit the selection of the identity of the first excited microphone (this was predictable since the aircraft flew a prescribed path); this avoided getting locked into an improper data acquisition sequence.

Thus, at the end of one multimicrophone cycle, each counter would be stopped at some time with respect to the first counter stimulated. The busy bit was generated when any counter was counting. The transition to busy cued the Analog-to-Digital Converter to converge and the transition to not busy cued the computer to first, accept the data from the counters and, second, test end-of-conversion until the digitization was ready for transfer.

The computer sampled the data asynchronously, buffering sufficient data to reform the polar signatures. The computer terminal was used to periodically enter the aircraft type, flight mode and temperature (to calculate the velocity of sound). The program did the rest, listing the results on the line printer as per the funder's preference.

CONCLUSION

Figure 7 illustrates the format of the data as reported and figure 8, the graphical representation. It was found that this technique worked extremely well on a variety of aircraft whether the blade slap was particularly audible or not. To date, it isn't clear whether a wind correcting algorithm will be possible for this technique but one will be persued with the interest of a funding organization. It was found, however, that in relatively still air, this signature technique is both cost effective and timely.

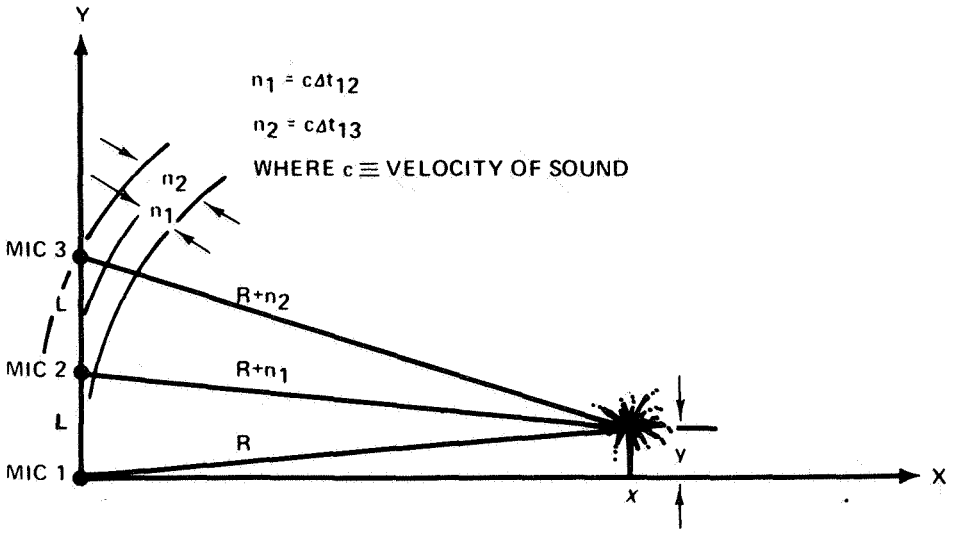

$R^2 = x^2+y^2$

$(R+n_1)^2 = x^2+(L-y)^2$

$(R+n_2)^2 = x^2+(2L-y)^2$

Figure 1.- 3 microphone vertical array.

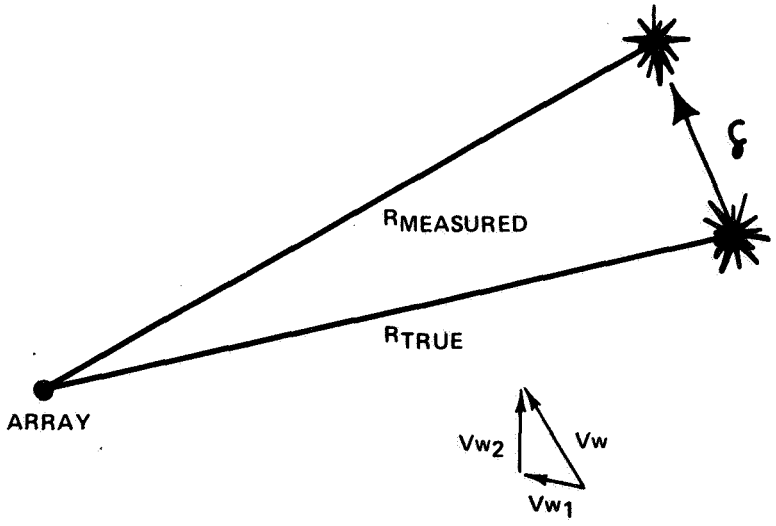

$T_{PROPAGATION} = R_{MEASURED}/V_S$

$\zeta = (V_w)\,(T_{PROPAGATION})$

Figure 2.- Plan view of 3 microphone array in wind.

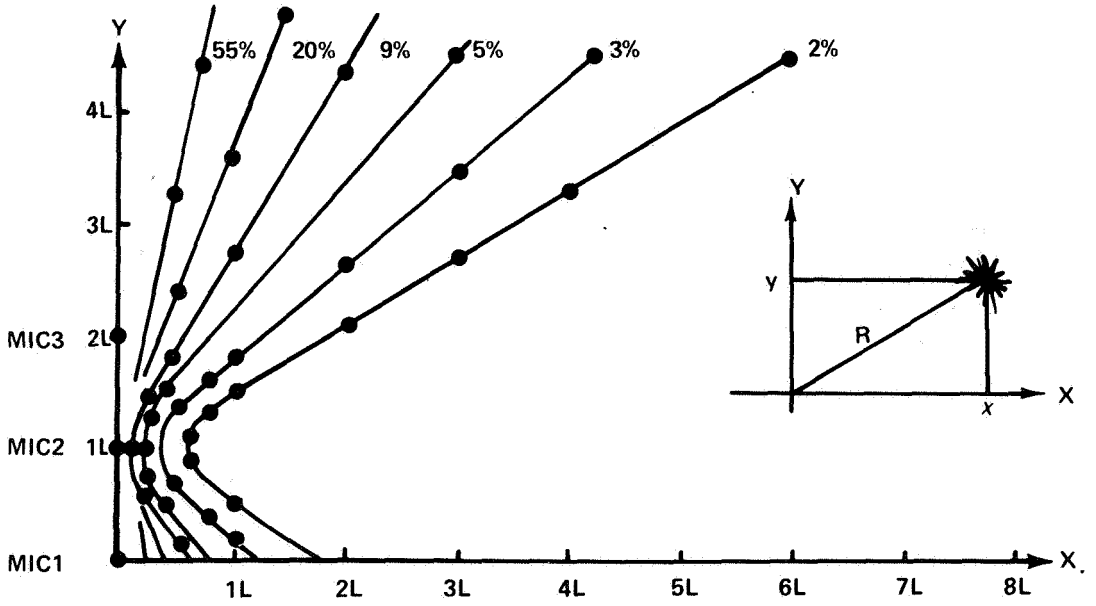

Figure 3.- Error in x caused by 1% error in V_s.

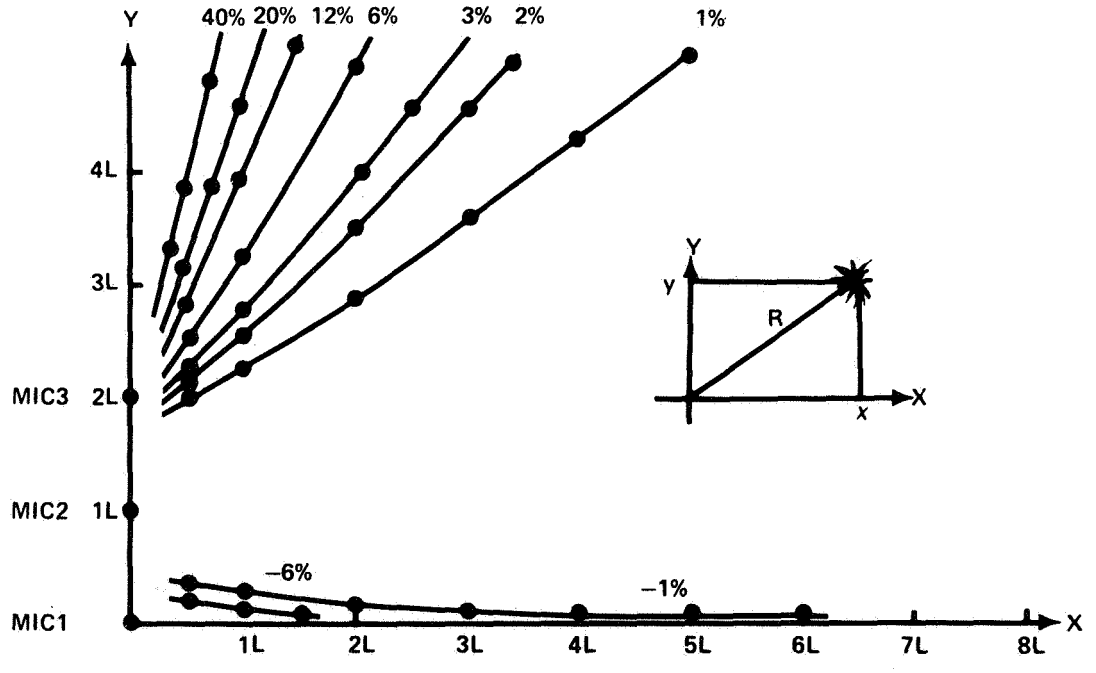

Figure 4.- Error in y caused by 1% error in V_s.

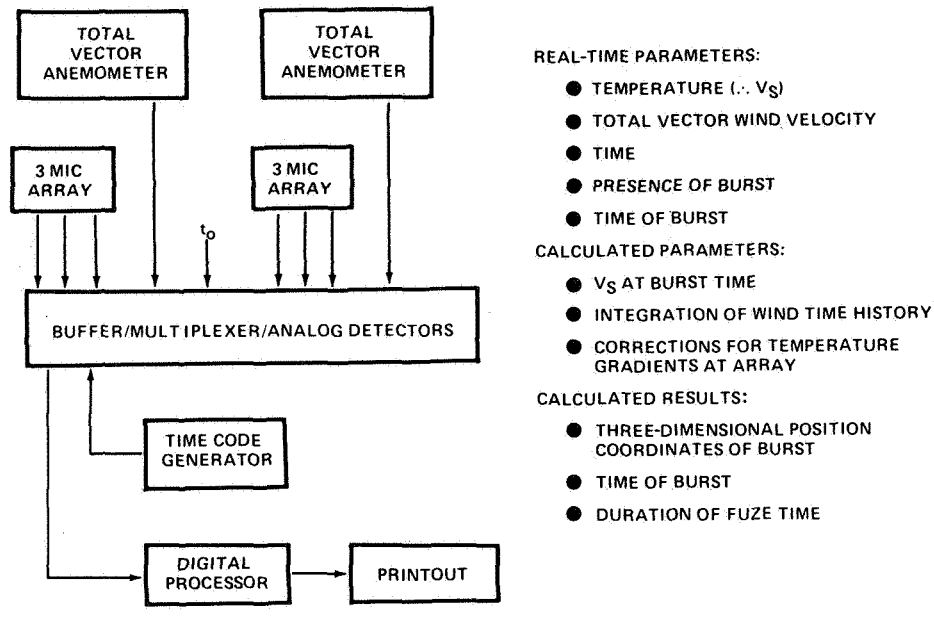

Figure 5.- Real-time sound ranging block diagram.

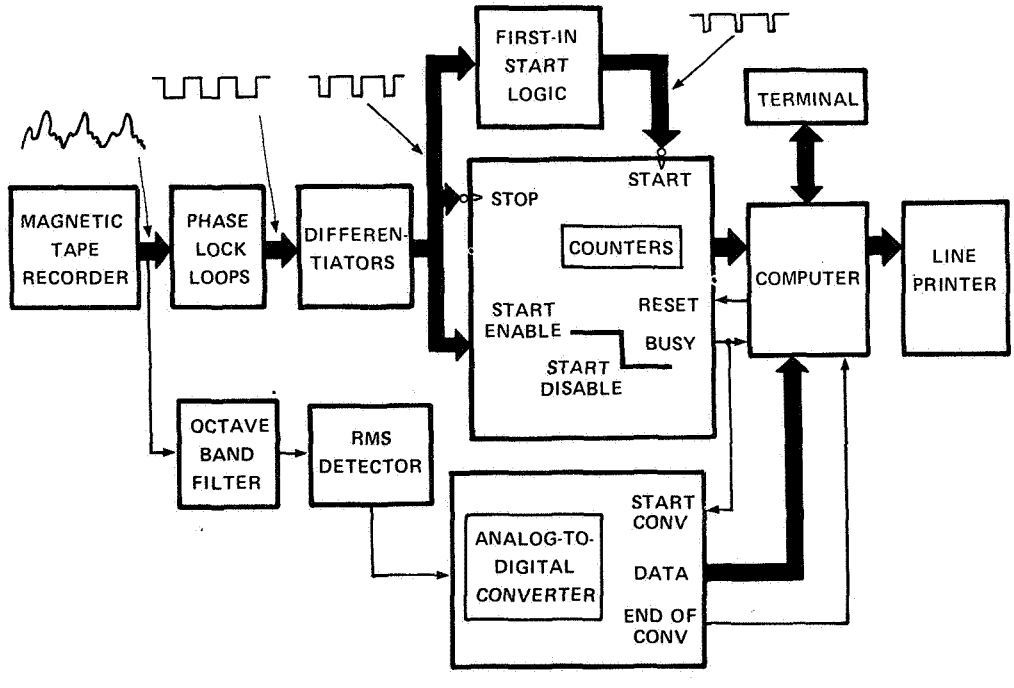

Figure 6.- Data processing system block diagram.

AMBIENT NOISE LEVEL 53.80 dB RUN NUMBER 1

THETA	SPLC	SPLR	SPLATT	SPLU
14.84	81.37	20.86	0.0	60.51
20.08	78.28	18.32	0.0	59.97
25.32	79.01	16.41	0.0	62.60
30.38	75.97	14.95	0.0	61.01
39.60	74.72	12.94	0.0	61.77
45.73	77.68	11.93	0.0	65.75
50.12	78.95	11.93	0.0	67.62
59.74	81.54	10.30	0.0	71.24
63.95	79.51	9.96	0.0	69.55
68.37	84.13	9.66	0.0	74.47
75.93	84.10	9.29	0.0	74.81
79.38	85.07	9.18	0.0	75.89
84.94	87.45	9.06	0.0	78.38
90.00	89.40	9.03	0.0	80.37
95.06	88.02	9.06	0.0	78.96
100.62	88.63	9.18	0.0	79.45
104.07	88.04	9.29	0.0	78.74
111.63	87.49	9.66	0.0	77.83
116.05	87.49	9.96	0.0	77.53
120.26	85.28	10.30	0.0	74.98
129.88	83.48	11.33	0.0	72.51
134.27	83.13	11.93	0.0	71.20
140.40	81.69	12.94	0.0	68.75
149.62	78.02	14.95	0.0	63.06
154.68	75.28	16.41	0.0	58.87
159.92	71.41	18.32	0.0	53.09
165.16	72.63	20.86	0.0	51.77

Figure 7.- Typical computer printout.

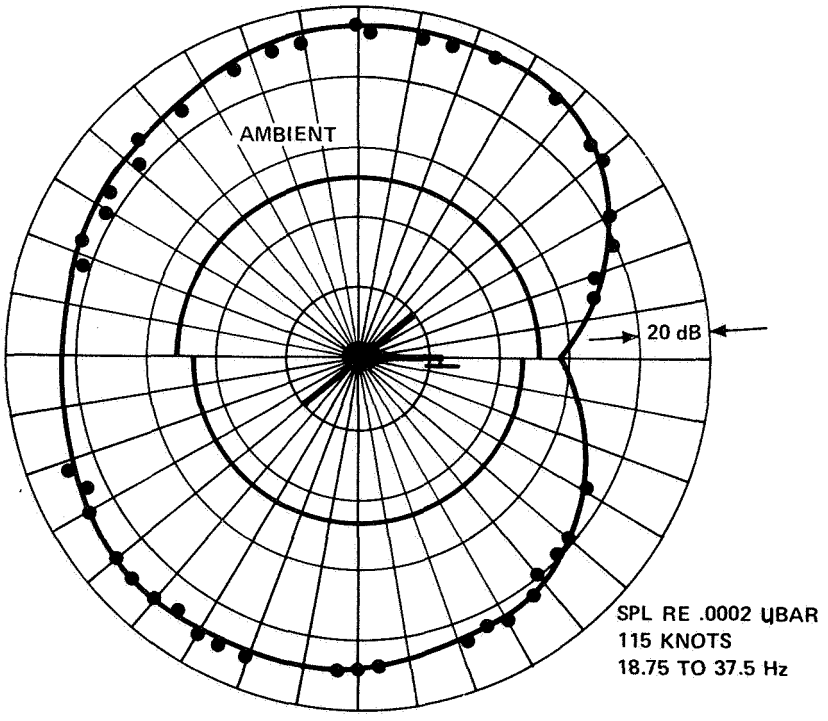

Figure 8.- Typical polar plot.